Dynamic Crack Processes via Molecular Dynamics

S. J. Zhou,[1] P. S. Lomdahl,[1] R. Thomson,[2] and B. L. Holian[1]
[1]*Theoretical Division and Center for Nonlinear Studies, Los Alamos National Laboratory, Los Alamos, New Mexico 87545*
[2]*Materials Science and Engineering Laboratory, National Institute of Standards and Technology, Gaithersburg, Maryland 20899*
(Received 11 October 1995)

From large-scale molecular-dynamics simulations of dynamic crack propagation, we find that cracks accelerate quickly to a relatively steady velocity. Energy released by bond breaking accumulates in a local phonon field that moves with the crack tip and promotes the emission of dislocations. Branching follows dislocation emission along a slip plane. The branching instability requires the crack to achieve a critical velocity, as well as an induction time for energy buildup at the crack tip.

PACS numbers: 61.72.Lk, 61.72.Yx, 62.20.Fe, 62.20.Mk

Fracture of materials is essentially a dynamic process, at least in the final stage. In this paper, we will show that understanding complex processes such as crack branching and dislocation emission from a dynamic crack requires realistic treatment of the truly atomistic dynamics.

In the earlier literature [1], dynamic instability was not seriously addressed. Attention became focused on the phenomenon, however, by recent experimental studies [2], and several theoretical attempts have followed [3–6]. The lattice theory of Marder and Liu [4] exhibits crack branching at a critical velocity, although it does not distinguish between branching and dislocation emission.

With the advance of computer power and efficient molecular-dynamics (MD) numerical techniques, the full dynamical and atomistic nature of this problem can be revealed. However, there are two major limitations in investigating dynamic fracture, even with massively parallel, multimillion atom MD [7,8]: small computational system sizes (submicrometer) and short time scales (nanoseconds). The strain fields associated with a crack are long range in character, and the stress waves generated by a propagating crack need special treatment to prevent them from reflecting from free surfaces and returning to disturb the behavior of the crack. Holian and Ravelo have developed an efficient atomistic boundary treatment using ramped viscous damping to absorb sound waves generated at crack tips [7]. We have considerably improved the delicacy of MD simulations of fracture by using these impedance-matched acoustic-absorbing reservoirs and by initially embedding an atomistically sharp equilibrium crack (i.e., loaded at the critical Griffith value), displacing atoms according to continuum elasticity, and then applying a small overstrain to gently drive the crack.

In this paper, we simulate a 2D model triangular lattice where atoms interact via a Morse pair potential, $\phi(r) = e^{-2\alpha(r-1)} - 2e^{-\alpha(r-1)}$, where we use as units the distance r_0 between neighbors in the zero-temperature and zero-pressure crystal and bond energy ε. For $\alpha = 6$, the Morse and Lennard Jones 6-12 potentials are almost indistinguishable; copper can be crudely described by $\alpha \approx 3.5$. To make both the potential energy and the force decay smoothly to zero at $r = r_{\max} = 2.5r_0$, we multiply the Morse function for $r_0 < r < r_{\max}$ by $w(r) = [1 - (\frac{r-r_0}{r_{\max}-r_0})^3]^2$. For $\alpha = 7$, the longitudinal c_l, transverse c_t, and Rayleigh c_R sound speeds (linear in α) are 10.5, 6.1, and 5.6 in units of $(\varepsilon/m)^{1/2}$. The unit of time t_0 in these calculations is determined from $\varepsilon = mr_0^2/t_0^2$, where m is the atomic mass; the computational time step in the Stoermer centered-difference integration of the MD equations of motion was chosen to be $\Delta t = 0.02t_0$. The initial temperature of the system was set to nearly zero, namely, $T_0 = 10^{-6}\varepsilon/k$.

Our computational cell with a sharp equilibrium crack and viscous damping ("stadium") boundaries is depicted in Fig. 1. The system studied consists of long rectangular samples with aspect ratio (horizontal/vertical length) of 5 or 6. Systems with more than 400 000 atoms are sufficiently large to take care of the long-range character of crack strain fields. The shortest half crack length of the sharp initial crack is $240r_0$, which is long enough that the waves generated at one crack tip can reach the other tip only after the initiation of branching. (For the Morse potential with $\alpha = 7$, this delay is $\sim 48t_0$; all the data reported in this paper are obtained before this time.) We absorb sound waves and mobile dislocations in a smooth way by ramping up the viscous damping coefficient γ in a region at least 20 atomic layers thick surrounding the central elliptical sample (wherein standard Newtonian mechanics applies). The Hamiltonian equations of motion for all N coordinates $\mathbf{r}$ and thermal velocities $\mathbf{u}$ are given by $\dot{\mathbf{r}} = \mathbf{u} + \dot{\epsilon}x\hat{\mathbf{x}}$ and $\dot{\mathbf{u}} = \mathbf{F}/m - \dot{\epsilon}u\hat{\mathbf{x}} - \gamma\mathbf{u}f$, where the elliptical stadium function f is zero inside and $0 \le f \le 1$ outside:

$$f(\mathbf{r}) = \min\left(1, \max\left(0, \frac{(x/L_x)^2 + (y/L_y)^2 - (a/L_x)^2}{1/4 - (a/L_x)^2}\right)\right).$$

 0031-9007/96/76(13)/2318(4)$10.00

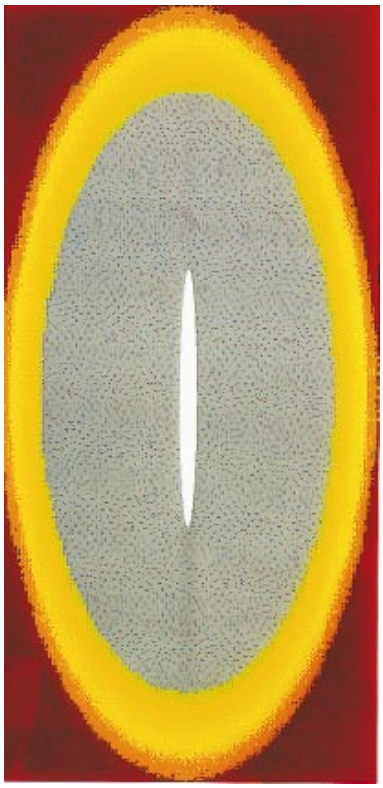

FIG. 1. (color) Schematic of the molecular-dynamics computational cell colored by the stadium function $f(x, y)$.

L_x and L_y are the widths of the entire computational cell and a and b are the x and y axes of the inner sample region, such that $a/L_x = b/L_y$. Outside the stadium the viscous damping coefficient [7] builds up to a maximum value, which at zero thermal bath temperature ($T_0 = 0$) critically damps sound waves at the root-mean-square Einstein frequency ω_E (= 17.2 for the Morse $\alpha = 7$): $\gamma = 2\omega_E(1 - T_0/T)$. The temperature T measured in the reservoir region is $kT = \sum m(u^2 + v^2)f/(2\sum f)$ (the sum is over all N atoms). These equations of motion allow homogeneous expansion [7] in the x direction for a vertical crack, at a strain rate given by $\dot{\varepsilon}(t) = \dot{\varepsilon}(0)/[1 + \dot{\varepsilon}(0)t]$.

As shown by Holian and Ravelo [7], adding global viscous dissipation—particularly effective near the crack tip—could change the condition for dislocation emission. Global viscous damping has also been employed by Langer [3] in his continuum model. We emphasize that in the work reported here we employ damping *only outside* the sample region, in the absorbing reservoir. At $t = 0$, we apply a displacement field, corresponding to the remote loading strain ϵ_0 just below the Griffith (critical) fracture value ϵ_c, to the atoms initially at perfect lattice points, and then increase the strains by applying a homogeneous strain rate, where the boundaries parallel to the direction of a crack expand at constant velocity. For crack growth and dislocation nucleation, we can simulate similar physical processes to those in conventional experiments, provided that the overloading strain changes much more slowly than the process of crack motion and dislocation emission. For example, with $\dot{\epsilon} = 0.0001$, a pair of atoms separated by one lattice spacing r_0 will increase its separation by $0.0001r_0$ in the time of t_0, as compared to the much larger distance that the crack tip runs (about $2r_0$ under a typical maximum crack-tip velocity). This also means our constant strain-rate loading is very close to constant-displacement loading ("fixed grips").

We have performed calculations with various initial crack lengths l_c, strain rates $\dot{\epsilon}$, and Morse potential parameters α. We emphasize two principal observations: (1) decreasing α tends to make dislocation emission easier, and (2) increasing $\dot{\epsilon}$ causes a crack to branch sooner and makes its branching paths more chaotic. Table I gives the maximum crack-tip velocities for various strain rates and ratios η of crack size to sample area S: $\eta = 2\pi l_c^2/S$. We find that the maximum velocities increase with decreasing ratios of crack size to sample area. It is interesting to note that no branching is observed below $\sim 0.35c_R$, and those speeds with branching are very close to experimental values reported by Sharon, Gross, and Fineberg [2].

In Fig. 2, we present some of our results for crack-tip velocities as functions of time. Figure 2(a) shows cases where no crack branching was observed. For case A in Table I, the crack starts to run, reaches the maximum velocity, goes to zero velocity, retreats, and then moves forward again. We are thus able to fine-tune the dynamical crack behavior through the specimen geometry factor η and loading rate $\dot{\epsilon}$. In the cases of crack branching shown in Fig. 2(b), data are plotted up to the initiation of the first branch. Very accurate crack-tip positions can be obtained by monitoring the potential energy of each atom. For case F in Table I, the atoms first readjust their initial positions given by elastic theory. (The elastic solution is generally very accurate, except for a small region within about 3 lattice spacings around the crack tip.) At $t = 2.0$, the crack starts to propagate and quickly reaches the terminal velocity of about 1.7 ($= 0.36c_R$) at a time of $t = 6$. The dynamic crack has been unsuccessfully attempting to branch, which causes small oscillations in the crack-tip velocity. As it opens up, the dynamic crack tip gets more rounded in shape than the initial static one; the tendency for the crack to branch increases with time.

This finding of a delayed dynamic buildup is strikingly different from traditional theories that show that crack-tip velocity *uniquely* determines the behavior of a dynamic

TABLE I. Maximum crack tip velocity $v_{\max}$ in units of c_R for various Morse potential parameters α, ratios of crack size to sample area η, and strain rates $\dot{\epsilon}$.

	$l_c(t = 0)$	ϵ_0	α	η	$\dot{\epsilon}$	$v_{\max}$
A	480	0.00354	7	5.02	0.000005	0.18
B	480	0.00354	7	4.19	0.00001	0.26
C	240	0.00500	7	1.05	0.0001	0.34
D	240	0.00500	7	1.05	0.0005	0.36
E	240	0.00580	6	1.05	0.0005	0.36
F	240	0.00580	6	1.05	0.0001	0.36

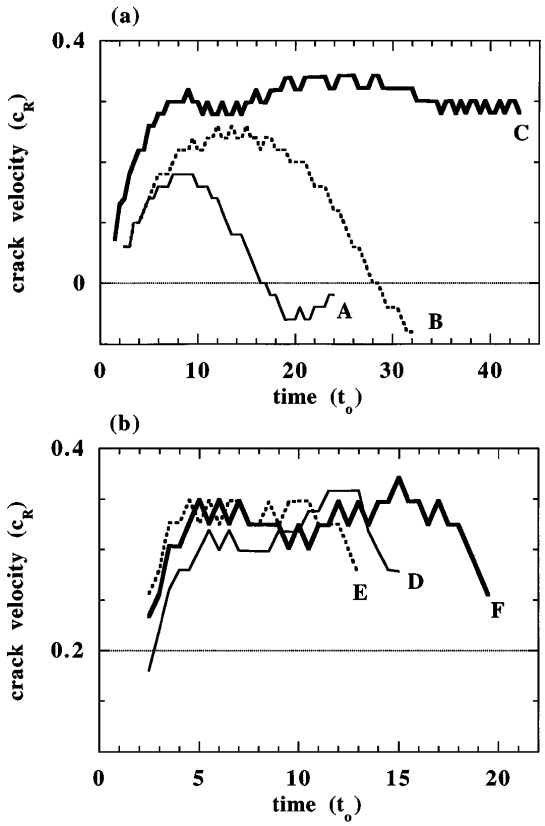

FIG. 2. The crack tip speed as a function of time (a) without crack branching, (b) with crack branching. Cases A–F are listed in Table I.

crack. Furthermore, the crack branching occurs at a significantly lower velocity than its maximum value. Clearly, the crack-tip velocity is *not* a sufficient condition to trigger the crack-branching instability. Instead, we find that the gradual accumulation of energy around the dynamical crack tip is an essential feature for the ultimate emission of dislocations and crack branching.

A principal finding of this paper is that the initial motion of the crack is very quiet and smooth, without dislocation emission or branching, but that gradually a region of excitation—the apparent source of the crack instability—builds up in the vicinity of the tip. This energy buildup is not a feature of the linear continuum theory of a crack [1], where the crack radiation field consists of a radiating front, behind which the stable (steady-state) crack stress field moves uniformly with the crack tip. (Langer's nonlinear continuum theory [3] also does not predict a delayed instability.) Thus this signal feature, a gradual buildup of excitation due to bond breaking during dynamic crack propagation, is an entirely atomistic phenomenon, suggesting that crack instability in crystals arises from the lattice character of the system. From movies of the particle velocity field, as well as the atomic force field (a snapshot of which is shown in Fig. 3 just prior to dislocation emission and crack-branching events), we see that the excitation spreads more slowly than the infinite-wavelength longitudinal sound speed, that the characteristic wavelength is finite (approximately five lattice spacings, as observed previously [7]), and that there are prominent directional features of shear motion along lattice slip planes (note the bowtie pattern on the butterfly in Fig. 3). Thus the excitation field which leads to instability in the propagation of a dynamic crack is not at all a set of random thermal fluctuations, but rather a more coherent localized set of phonons. We are in the process of analyzing in more detail the nature of this excitation field, including how it relates to lattice trapping effects and to lattice models for propagation velocities [4].

We find that the local potential energy is the most useful way to show defect configurations such as crack surfaces and dislocation cores. The local potential energy clearly indicates the future growth paths of cracks or dislocations: In Figs. 4(a)–4(c) ($t = 2, 13.5, 21.5$), we see clearly the buildup of the potential energy associated with the localized as well as radiated phonon fields; and in Figs. 4(d)–4(f) ($t = 22.5, 25, 38$), we see that dislocations can be emitted from a "brittle" crack tip (defined here as a static crack tip that cannot emit a dislocation) when the crack runs sufficiently fast. Therefore, crack motion promotes dislocation emission. (How the dynamics of a crack, as well as the interatomic potential, influence dislocation emission criterion will be discussed in future work.)

It is found that crack branching is closely tied to dislocation nucleation and emission. In Fig. 4(d), one dislocation, nucleated at the right side of the crack tip (at $t = 22$), is then ejected $2r_0$ away from the crack tip along the $-60°$ slip plane. In Fig. 4(e), the crack tip starts to branch along the slip plane of the emitted dislocation, and the branch closely follows the dislocation motion.

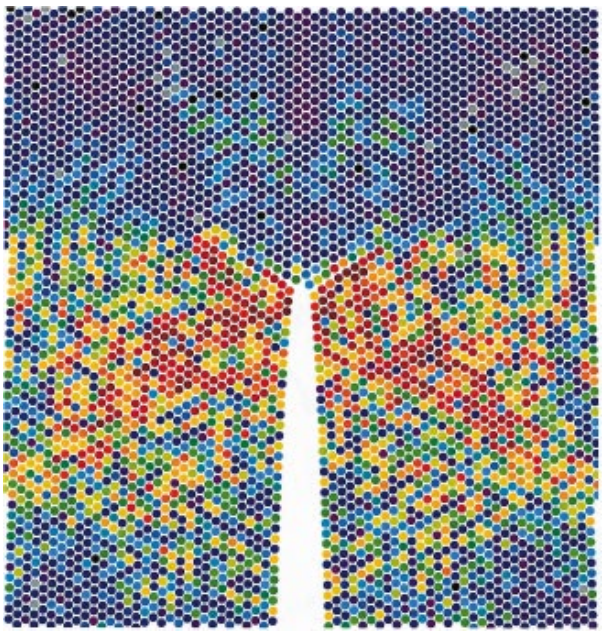

FIG. 3. (color) Dynamic crack just before dislocation emission and crack branching ($t = 21.5$) for case F, represented by atomic forces (red indicating the highest magnitude).

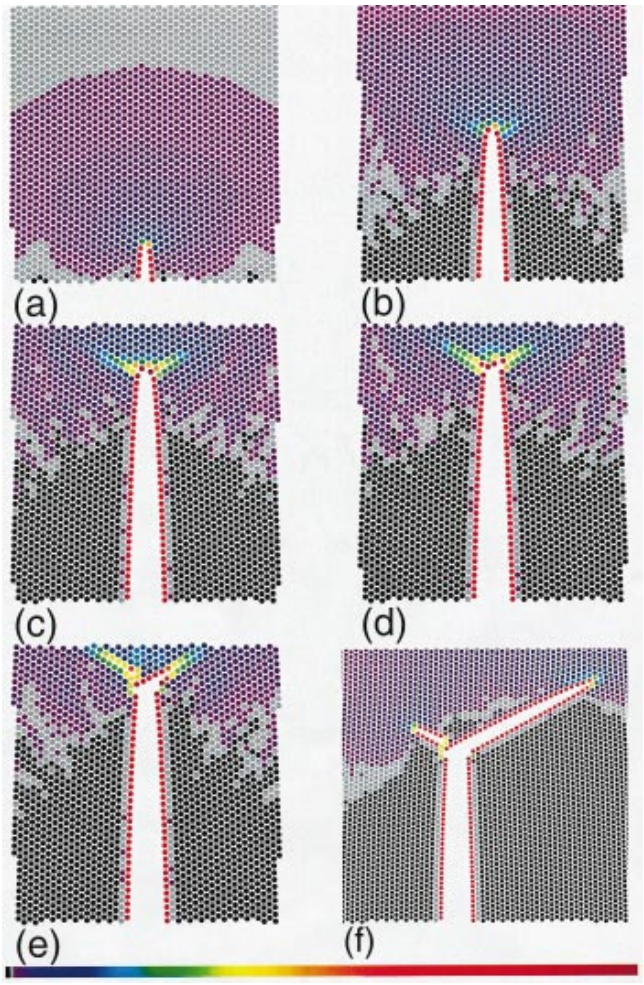

FIG. 4. (color) Dynamic crack propagation sequence represented by local potential energy (range of -3.1 to -1.4 indicated by color bar, left to right).

A similar process of dislocation emission and crack branching also occurs along the $+60°$ slip plane a little bit later (about $t = 26.5$). These general features were observed by Holian and Ravelo [7], though admittedly under much cruder loading conditions than ours. A very similar phenomenon has been observed in transmission electron microscopy experiments [9].

As seen in Fig. 4(f), asymmetric branching can occur. This is understandable: The 2D triangular lattice is macroscopically isotropic, but not locally. The $+60°$ and $-60°$ slip planes are not symmetric relative to a crack tip, so it is impossible for a crack to branch completely symmetrically—the choice of path is made randomly. Once the crack tip has begun to branch along one of the two slip planes, the accumulated energy at the crack tip has been partially released, so that the possibility of growing immediately along the other slip plane is suppressed.

Changing the loading rate or the Morse potential parameter changes the branching pattern significantly. However, in all the cases we have observed the crack branching is triggered by dislocation emission, following the motion of the emitted dislocation.

Based on our results, we can now discuss what causes dynamic crack branching. The driving force for dislocation nucleation in a crystal increases with increasing crack-tip speed. For mode I loading in a 2D triangular lattice, dislocation nucleation occurs preferably along $\pm 60°$. Dislocation nucleation distorts the arrangement of the atoms near the slip plane emanating from the crack tip, thus increasing the elastic driving force for branching. It also creates a weak path for the crack to follow, by analogy with the fact that two blocks of crystal are easier to pull apart after they are sheared. Figures 3 and 4 have clearly shown that dislocation nucleation determines the initial crack branching path and angle. Once the crack branches and grows a few lattice spacings along the slip planes, the branching cracks gradually change their path so that the average paths have small angles relative to the original crack path, i.e., $\theta = 0$. This is because the distortions of the stress field caused by dynamic cracks gradually fade away, and therefore the stress field approaches that static one, which requires crack growth in the plane of $\theta = 0$. The smaller angle of crack branching observed in the experiments (due to limitations of resolution) are very possibly the average over the whole branching path, rather than just the first angle.

Our simulations indicate that the crack velocity is a necessary, but *not* sufficient, condition for crack branching. This is different from existing continuum and lattice theories, where a critical crack velocity is used as the only indicator for crack branching. As shown in Fig. 2 and Table I, a dynamic crack cannot branch when its maximum velocity is below $0.35c_R$. On the other hand, for those cracks with high enough maximum velocity, branching occurs not at the point of maximum velocity, but some time later, after the crack velocity has dropped below the maximum.

Computations were performed on CM-5 at the Advanced Computing Laboratory at Los Alamos. We thank A. Needleman, R. Ravelo, P. Gumbsch, W. G. Hoover, and J. Langer for helpful discussions and suggestions.

[1] L. B. Freund, *Dynamic Fracture Mechanics* (Cambridge University Press, New York, 1990).
[2] W. G. Knauss and K. Ravi-Chandar, Int. J. Fract. **27**, 127 (1985); J. Fineberg, S. P. Gross, M. Marder, and H. L. Swinney, Phys. Rev. Lett. **67**, 457 (1991); E. Sharon, S. P. Gross, and J. Fineberg, Phys. Rev. Lett. **74**, 5096 (1995).
[3] J. S. Langer, Phys. Rev. Lett. **70**, 3592 (1993).
[4] M. Marder and X. Liu, Phys. Rev. Lett. **71**, 2417 (1993).
[5] X.-P. Xu and A. Needleman, J. Mech. Phys. Solids **42**, 1397 (1994).
[6] E. S. C. Ching, Phys. Rev. E **49**, 3382 (1994); E. S. C. Ching, J. S. Langer, and H. Nakanishi, Phys. Rev. E **52**, 4414 (1995).
[7] B. L. Holian and R. Ravelo, Phys. Rev. B **51**, 11 275 (1995).
[8] D. M. Beazley and P. S. Lomdahl, Paral. Comp. **20**, 173 (1994).
[9] S. M. Ohr, Scr. Metall. **20**, 1501 (1986).